HardwareX 10 (2021) e00204

Contents lists available at ScienceDirect

HardwareX

journal homepage: www.elsevier.com/locate/ohx

A low-cost, wearable, do-it-yourself functional near-infrared spectroscopy (DIY-fNIRS) headband

Francis Tsow [a,b,1], Anupam Kumar [a,b,1], SM Hadi Hosseini [c], Audrey Bowden [a,b,d,*]

[a] Biophotonics Center, Vanderbilt University, Nashville, TN 37232, United States
[b] Department of Biomedical Engineering, Vanderbilt University, Nashville, TN 37232, United States
[c] Department of Psychiatry and Behavioral Sciences, Stanford University School of Medicine, Stanford, CA 94305, United States
[d] Department of Electrical Engineering, Vanderbilt University, Nashville, TN 37232, United States

ARTICLE INFO

Article history:
Received 26 October 2020
Received in revised form 14 May 2021
Accepted 16 May 2021

Keywords:
Functional near infrared spectroscopy
Neuroimaging
Hemodynamics
Brain imaging

ABSTRACT

Neuromonitoring in naturalistic environments is of increasing interest for a variety of research fields including psychology, economics, and productivity. Among functional neuromonitoring modalities, functional near-infrared spectroscopy (fNIRS) is well regarded for its potential for miniaturization, good spatial and temporal resolutions, and resilience to motion artifacts. Historically, the large size and high cost of fNIRS systems have precluded widespread adoption of the technology. In this article, we describe the first open source, fully integrated wireless fNIRS headband system with a single LED-pair source and four detectors. With ease of operation and comfort in mind, the system is encased in a soft, lightweight cloth and silicone enclosure. Accompanying computer and smartphone data collection software have also been provided, and the hardware has been validated using classic fNIRS tasks. This wear-and-go design can easily be scaled to accommodate a larger number of fNIRS channels and opens the door to easily collecting fNIRS data during routine activities in naturalistic conditions.

Specifications table

Hardware name	Do-it-yourself functional near-infrared spectroscopy (DIY-fNIRS) headband
Subject area	• Psychology • Neuroscience • Educational Tools and Open Source Alternatives to Existing Infrastructure
Hardware type	• Measuring physical properties and in-lab sensors • Field measurements and sensors • Electrical engineering and computer science
Open Source License	Creative Commons Attribution-ShareAlike license
Cost of Hardware	$215
Source File Repository	http://doi.org/10.17605/OSF.IO/AG46P

* Corresponding author at: Biophotonics Center, Vanderbilt University, Nashville, TN 37232, United States.
E-mail address: a.bowden@vanderbilt.edu (A. Bowden).
[1] These authors contributed to the work equally.

https://doi.org/10.1016/j.ohx.2021.e00204
2468-0672/

1. Hardware in context

Better understanding of how the brain works in naturalistic environments (e.g., at home, work, or while performing an activity that is typically done outside of the laboratory) can have tremendous impact on the fields of psychology, physiology, behavior science, economics and productivity [1–4]. Functional neuroimaging is a general term for technologies that spatially map brain activity over time. Such technologies include functional magnetic resonance imaging (fMRI), positron emission tomography (PET), electroencephalography (EEG), and functional near-infrared spectroscopy (fNIRS). Unfortunately, most of these technologies are not well adapted for use in naturalistic environments [5]. For example, fMRI and PET are bulky, expensive, and require immobilization of subjects; thus, they can only be used in a laboratory or clinical setting to test a limited number of activities. EEG and fNIRS systems are typically smaller and more economical; thus, they can assess a broader range of activities. However, portable EEG technology typically suffers from poor spatial resolution and susceptibility to motion artifacts. Among these neuromonitoring options, fNIRS provides the best compromise: acceptable tolerance to motion artifacts, good spatial (cm) and temporal resolutions (8 to 10 Hz) and portability [6,7].

fNIRS systems consist of light sources and detectors placed on the scalp to quantify relative changes in oxygenated and deoxygenated hemoglobin in different cortical regions. A single channel for fNIRS sensing is typically referred to as an "optode" and consists of a light source and a detector. A light source may be shared by multiple detectors and vice versa to create multiple sensing channels without adding components. The distance between a source and detector controls the depth of imaging, and source-detector distances can be as little as 5 mm to 10 mm ("short channel") for detecting and correcting shallow physiological signals or motion artifacts *not* from the brain [1,8–11] or as much as 20 to 60 mm ("long channel") [10–13] for detecting hemodynamic activity in the brain. Source-detector distances for "long channels" are selected based on the light source and how deep a user wishes to image into brain tissue: low-cost LED sources have a low depth of penetration in tissue and are used with shorter source-detector distances of 20 to 35 mm, and expensive laser-based sources have greater depth of penetration in tissue and can image deeper into the brain with larger source-detector separations [1,13]. Light source wavelengths are typically selected in near-infrared pairs, wherein the first source ranges from 650 nm to 750 nm and the second source is above 820 nm [14]. Recently, three-wavelength fNIRS systems speculating detection of analytes other than hemoglobin such as water [15] or cytochrome C-oxidase [16,17] have also been developed to either improve calculations of changes in hemoglobin concentrations or to utilize an alternate biomarker for cerebral activity. Three wavelengths have also been used for hemoglobin-only systems, where the third wavelength is selected at a point such as 805 nm, close to the isobestic point of hemoglobin [18,19]. However, most commercial and research systems utilize two wavelengths for their studies. Since our system was intended to be as low-cost as possible, we only utilized two LEDs at 740 nm and 850 nm.

A number of studies have demonstrated the potential use of fNIRS in naturalistic environments using either commercial or custom wearable systems capable of wirelessly transmitting hemodynamic neuromonitoring data to an external device [1,2,4,20–23]. Companies such as Artinis [24] market wireless whole-brain wearable fNIRS cap systems, and research groups such as Von Lühmann et al. [25,26] and Zimmerman et al. [27] ("NinjaNIRS") have even made their wireless fNIRS hardware designs open source. Unfortunately, large component enclosures and exposed cabling interfacing their subcomponents (source or detector probes, data acquisition circuitry, and broadcasting microcontrollers) have frequently rendered such designs susceptible to damage during use in naturalistic conditions [1,4,11,28–31]. Recently, fully integrated and portable head-mounted systems have been designed by companies such as OBELAB and Newman Brain, which fully enclose all system subcomponents (enclosures, cabling, and electronics) inside headgear shaped similarly to virtual reality (VR) devices. Such systems provide multiple advantages: lower dependence on skilled experts for experimental setup, reduced susceptibility to damage, and easy-to-use accompanying software. Unfortunately, no fully integrated open source systems have been made available to the fNIRS research community. Additionally, available fully integrated systems also struggle from sizeable weight (OBELAB NIRSIT-Lite: 190 g [32], OBELAB NIRSIT: 550 g [33], NewmanBrain, 290 g [34]), which makes them uncomfortable to use over a long period of time.

In this manuscript, we describe a scalable prototype of a low-cost, lightweight, and wireless single-channel fNIRS headband platform that is easy to assemble and use for neuroimaging studies in naturalistic conditions. We have designed single-channel fNIRS hardware and accompanying data collection software (for Android phones and Windows/Mac Computers) that can be assembled for approximately $215. In addition to collecting fNIRS signals, the system can reduce artifacts due to motion and other superficial signals [10,11,13]. We demonstrate the use of this technology to yield reliable results during various fNIRS maneuvers including a breath-holding test, which is known to modulate cortical hemodynamics and is commonly used to validate fNIRS systems.

2. Hardware description

The technical objective of this manuscript is to lay the foundation for a fully integrated fNIRS headband that is 1) easy for researchers to assemble, 2) simple for research subjects to use at home, and 3) affordable for most users. To meet the first objective, ease-of-assembly and future scalability were adopted as guiding principles in the design process. For the second,

anticipated requirements for usability in the home environment were considered, such as child-friendliness and tolerance to mechanical wear and tear, by using cushioning and maximizing use of soft and conformal materials.

The complete hardware system consists of multiple subcomponents: electro-optical components for fNIRS sources and detectors, control electronics for data acquisition and wireless broadcasting, and a lightweight conformal enclosure.

Electro-optical components were chosen as functions of the optical properties, form factor, and cost required to achieve fNIRS signals. For the source of our system, an LED pair consisting of light at 740 nm and 850 nm was selected based on the absorption spectra of oxy- and deoxy-hemoglobin on either side of where the spectra intersect ("isobestic point"). The chosen near-infrared wavelength LEDs has an output radiant intensity not more than 3 mW, which is below the IEC (International Electrotechnical Commission) 60825-1 suggested limit, assuming an area of >2 mm^2. Both LEDs also have relatively narrow spectral bandwidths with peak emission wavelengths at 740 nm and 850 nm with aberrations of approximately ±30 nm at 20% of their peak intensities. For the detector, a silicon photodiode was selected with a spectral sensitivity bandwidth encompassing the wavelengths of interest. The dark current of the photodiode is specified to be 2 nA at room temperature. A voltage follower circuit and current-to-voltage conversion circuit are used to activate the LEDs and read the signal detected from the photodiodes, respectively. Both circuits can alternatively be built using low-power, low-noise transimpedance op-amps such as those by Texas Instruments (OPA2380 or OP2377).

The control electronics for this system were designed for modularity and ease of scalability by any member of the fNIRS community. Unfortunately, not all members of this community have the expertise in hardware engineering necessary to adapt fNIRS technology to their unique experimental requirements. Hence, a divide-and-conquer approach to the design was adopted: three ultra-low-power microcontrollers by Texas Instruments® were selected to manage data-acquisition, LED intensity, and system timing, respectively. The analog-to-digital converter (ADC) of the data-acquisition microcontroller is a 12-bit linear successive-approximation-register (SAR) ADC typically used for data acquisition. The aggregated data are wirelessly transmitted through a peripheral Bluetooth® Serial system-on-a-chip device by Microchip®. Dividing responsibilities across multiple controllers allows the system to be easily scaled up for future endeavors since the firmware development process becomes simpler for any non-engineering professional (or early-career engineers) to learn and customize without needing to learn complex firmware technologies for multitasking on embedded systems. Unsharing of the computational load also enables advanced audiences to add other sensors (e.g., accelerometers) and manage the distribution of system weight over different parts of the head to maximize comfort. The interconnectivity of the subcomponents of the circuit is represented in Fig. 1A.

For demonstration purposes, the assembled system presented in this manuscript consists of a single near-infrared LED pair (740 nm and 850 nm) and four silicon photodiode detectors placed collinearly at distances of 5 mm, 10 mm, 23 mm,

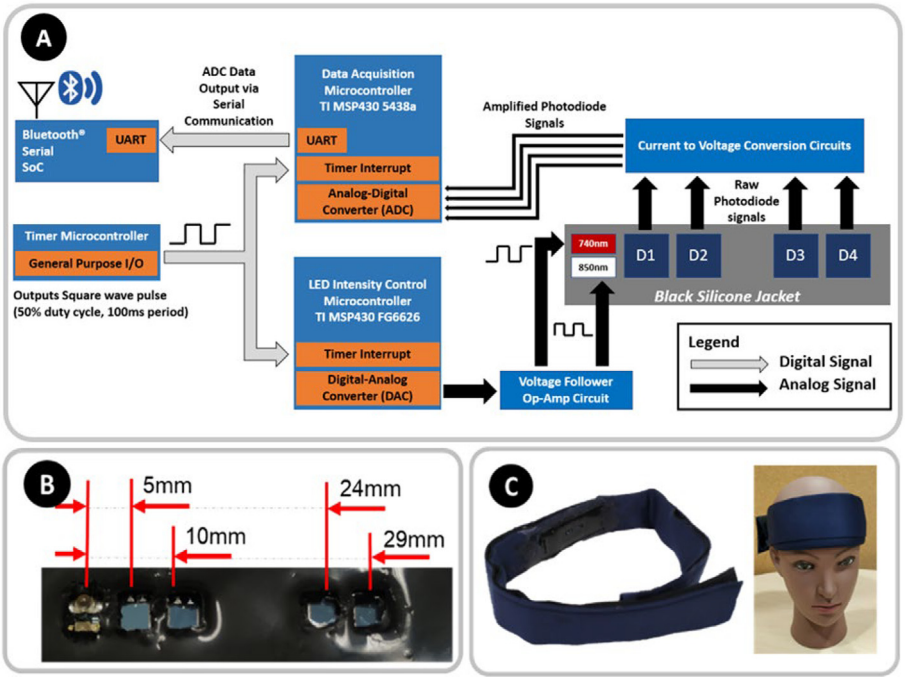

Fig. 1. A) Block diagram illustrating the interconnectivity of the various subcomponents constituting the fNIRS sensing control circuitry. B) Photograph (not to scale) of a prototype optode. C) Photograph showing a model wearing our fNIRS headband device.

and 28 mm (Fig. 1B). This layout of source and detectors was selected to facilitate future decision-making regarding short- and long-channel placement in a prospective multichannel fNIRS system. This system can be scaled up to include 10 detectors and three sets of LED sources, wherein a "set" would constitute a group of multiple sources which can be illuminated together.

The control electronics and electro-optical components are jacketed in a soft, conformal headband enclosure consisting of silicone and cloth components. The electro-optical components are jacketed inside molded silicone that is "glued-on" to a laser-cut cloth. The remaining control electronics and battery are connected to the electro-optical components with flat and flexible cables (FFC) and are enclosed inside a pocket created by attaching folds of the cloth enclosure using Velcro®.

Once fully assembled (Fig. 1C), our open source fNIRS headband broadcasts data at 10 Hz, weighs only 142 g and has a battery life of up to 5 h (peak current consumption of 84 mA, tested using a 400-mAh lithium-ion polymer, LiPo, battery). The system unit cost is approximately $215 in single-unit volume and is expected to be significantly lower when it is mass-produced. This device has the following advantages for research:

- The device will allow home-based use
- The device will allow large-scale studies
- The device will allow long-duration studies (hours)
- The device will allow longitudinal studies
- The device will allow treatment response feedback and optimization
- The device will allow discovery of new fNIRS applications and knowledge

3. Design files

Design file name	File type	License Type	File Location
circuitDesigns	ExpressPCB circuit file	CC – sa*	*OSF*
circuitSchematics	Image file for circuitSchematics	CC – sa*	*OSF*
timerMCU	IAR embedded workbench project	CC – sa*	*OSF*
sourceIntensityControlMCU	IAR embedded workbench project	CC – sa*	*OSF*
dataAcquisitionMCU	IAR embedded workbench project	CC – sa*	*OSF*
sw_collectDataMATLAB	MATLAB® AppDesigner project	CC – sa*	*OSF*
sw_collectDataCpp	Visual Studio (C++) project	CC – sa*	*OSF*
sw_collectDataAndroid	Visual Studio (Xamarin.Android C#) project	CC – sa*	*OSF*
3D_CAD_SiliconeMold	Autodesk Inventor file	CC – sa*	*OSF*
2D_CAD_ClothEnclosure	LibreCAD file	CC – sa*	*OSF*

*Creative Commons Attribution-ShareAlike license

circuitDesigns: ExpressPCB PCB schematic (.sch) and design files (.pcb) with multiple circuits to be cut out along dotted lines on the silk screen.

timerMCU: IAR Embedded Workbench Firmware project for programming a MSP430F2001 microcontroller to output timing signals to trigger interrupt events in other microcontrollers.

ledIntensityMCU: IAR Embedded Workbench Firmware project for programming a MSP430FG6626 microcontroller to control LED activation sequences. Additional functionality for controlling LED intensity and reading its digital-to-analog converters is also provided.

dataAcquisitionMCU: IAR Embedded Workbench Firmware project for programming the main MSP430F5438A microcontroller, which communicates with both the MSP430FG6626 microcontroller and Bluetooth System-on-a-Chip to wirelessly broadcast data. It is responsible for analog-to-digital conversion of the photodiode signal in synchrony with LED pulsing as guided by timer signals.

sw_collectDataCpp: A bare-bones 2017 Visual C++ program developed to receive and parse through raw wireless Bluetooth® for fNIRS data broadcasted from the fNIRS device.

sw_collectDataAndroid: An Android application and code for plotting and storing real-time data from the fNIRS device. Additionally, the GUI can be used to annotate when a stimulus is provided to the data.

sw_collectDataMATLAB: A MATLAB® GUI application for collecting and storing real-time data from the fNIRS device. Additionally, the GUI can be used to annotate when a stimulus is provided to the data.

3D_CAD_SiliconeMold: An Autodesk Inventor file for making the mold used for enclosing the optodes in soft silicone.

2D_CAD_ClothEnclosure: A LibreCAD file used as the input for the laser cutter to cut the cloth headband that holds the circuits and silicone-jacketed electronics in place.

4. Bill of materials

4.1. List of Electronic subcomponents

Designator on PCB	Description	Manufacturer	Part Number	Qty	Unit Cost	Total Cost
C1, C2	100 pF capacitor	KEMET	C0603C101J3GACTU	2	$ 0.15	$ 0.30
C3, C4, C5, C6	18 pF capacitor	Vishay Vitramon	VJ0603A180JXACW1BC	6	$ 0.12	$ 0.72
C7, C8	12 pF capacitor	Yageo	CC0603JRNPO0BN120	2	$ 0.10	$ 0.20
C9, C13, C17	1 μF capacitor	Vishay Vitramon	VJ0603Y104KXAAC	3	$ 0.34	$ 1.02
C10, C11, C15, C16	18 pF capacitor	Vishay Vitramon	VJ0603A180JXACW1BC	2	$ 0.12	$ 0.24
C12	0.1 μF capacitor	Vishay Vitramon	VJ0603Y104KXAAC	1	$ 0.34	$ 0.34
C14	1 nF capacitor	KEMET	C0603C102K4RECAUTO	1	$ 0.19	$ 0.19
D1, D2, D3, D4	Photodiode	Vishay	VBPW34S	5	$ 1.19	$ 5.95
D5	850 nm LED source	Wurth	15412085A3060	1	$ 0.53	$ 0.53
D6	740 nm LED source	Marktech	MTSM0074-843-IR	1	$ 3.45	$ 3.45
J1	2.54 mm pitch male headers for assembling programming pins	Samtec Inc.	TSW-150-07-T-S	9	$ 2.18	$ 19.62
J2	10-pin FFC cable connector	Molex	522,071,033	2	$ 1.16	$ 2.32
R1	1 MOhm resistor	Yageo	RC0603FR-071ML	1	$ 0.10	$ 0.10
R2	5.1 MOhm resistor	Yageo	RC0603JR-075M1L	1	$ 0.10	$ 0.10
R3	20 MOhm resistor	Vishay Dale	CRCW060320M0JPEAHR	1	$ 0.48	$ 0.48
R4	50 MOhm resistor	Stackpole Electronics	HMC0603JT50M0	1	$ 0.42	$ 0.42
R5, R6, R10	47 kOhm resistor	Panasonic Electronic Components	ERJ-3GEYJ473V	4	$ 0.10	$ 0.40
R7, R9	200 Ohm resistor	Panasonic Electronic Components	ERJ-1GN0R00C	2	$ 0.10	$ 0.20
R8, R18	0 Ohm resistor	Stackpole Electronics Inc.	RMCF0603ZT0R00	2	$ 0.10	$ 0.20
U1, U4	Op-Amp for LED controller microcontroller	Texas Instruments	OPA2380	2	$ 2.41	$ 4.82
U2	Clock timer microcontroller	Texas Instruments	MSP430F2001	1	$ 1.38	$ 1.38
U3	LED intensity control microcontroller	Texas instruments	MSP430FG6626	1	$ 10.89	$ 10.89
U5	LDO voltage regulator	Texas Instruments	TPS73630DBVT	1	$ 2.30	$ 2.30
U6	Op-Amp for photodiode signal amplification	Texas Instruments	OPA2377	1	$ 1.60	$ 1.60
U7	Data acquisition microcontroller	Texas Instruments	MSP430F5438AIPZR	1	$ 7.01	$ 7.01
U8	Bluetooth 2.1 classic module	Microchip Technology	RN42N-I/RM	1	$ 15.73	$ 15.73
X2, X3	18 MHz crystal	Citizen Finedevice Co Ltd	HC-49/U-S18000000ABJB	2	$ 0.66	$ 1.32
W1	6 pos 10″ FFC cable with 1.00 mm pitch	Assmann WSW Components	AFFC-100-06-254-11	2	$2.27	$ 4.54

(*continued on next page*)

(*continued*)

Designator on PCB	Description	Manufacturer	Part Number	Qty	Unit Cost	Total Cost
W2	10 pos 4″ FFC cable with 1.00 mm pitch	Molex	152,670,251	1	$1.86	$ 1.86
B1	Lithium-Polymer battery	Adafruit Industries	1578	1	$7.95	$ 7.95
B2	LiPo charger	SparkFun Electronics	PRT-10217	1	$8.95	$ 8.95
PCB	Single PCB to be cut and separated into pieces	ExpressPCB	Miniboard Pro	1	$100.00	$ 100.00
Total Electronics Related Costs						***$204.83***

Multi-use consumable supplies

Item	Description	Manufacturer	Part Number	Qty	Unit Cost	Cost
Dragon Skin FX-Pro (910 g)	2-Part silicone solution	Smooth-On, Inc.	SODragonskinfxprokit	28 g	$42.60	$1.71
Black Silicone Pigment (118 ml)	Black pigment for silicone	Smooth-On, Inc.	SilcPigBLACK4oz	7 ml	$34.95	$2.10
Ultimaker 3D Printing Material (750 g)	Black 2.85 mm PLA material	Ultimaker	1613	40 g	$49.95	$3.00
Polytechno Two Way Stretch Fabric (36″ x 60″)	1 square meter of 97% Polyester, 3% Spandex cloth to be laser-cut into headband enclosure	Shason Textile	WS-B436-424	0. 5	$4.97	$2.485
Total Multi-Use Consumables Cost						***$9.30***

**Cost values rounded up to two significant values*

Other equipment utilized

Item	Description	Manufacturer	Part Number	Cost
Ultimaker 3 3D printer	Desktop 3D printer	Ultimaker	B07YN8LTJ4	$3,850.00
PCB Cutter	Black pigment	Circuit Specialists	PCB CUTTER	$389.00
PLS6.75 Laser Cutter	Laser cutter	Universal Laser Systems	PLS6.75	$19,400.00
Total Equipment Cost (Multi-Use)				***$23,639***

6. Build instructions

The proposed wearable is an electro-mechanical assembly consisting of three subcomponents: control and sensing electronics, a silicone polymer skin, and a cloth and Velcro® casing. Once assembled, the wearable can be strapped the head of a user to broadcast fNIRS data to the Android Phone application or MATLAB® computer application provided. The assembly of the individual subcomponents and their integration are discussed below.

Control and sensing electronics

The control and sensing electronics consist of four small circuits for 1) power management, 2) LED control, 3) data acquisition, and 4) fNIRS sensing that require assembly by soldering relevant components and programming the microcontrollers. The data acquisition board also contains a Bluetooth® data module for broadcasting the fNIRS data. The fNIRS sensing circuits are two small circuits that are connected to each other using two small snippets of wire and to other circuits using cables. All circuits have been designed using ExpressPCB to fit onto a single, 4-layer printed circuit board (PCB) as a cost-savings mechanism; the board can be cut into individual circuits along the outline markers in the provided PCB file in the OSF repository. The fourth circuit (by Sparkfun®) is a detachable power management circuit that provides connection and charging to a LiPo battery.

The circuit components have been selected with both miniaturization and ease-of-assembly in mind. The components (integrated circuits, resistors, capacitors, cable connectors, etc.) need to be soldered onto their respective locations, which can be identified using the provided bill of materials (BOM) and the silk-screen layer of the provided PCB file. Additionally, it is also recommended that the PCBs be cut *prior* to soldering components onto them.

To functionalize the various microcontrollers in the circuit, they need to be programmed. In this project, programming entails either downloading a file to a microcontroller using a programmer device (U2, U3, U8) or wirelessly configuring a microcontroller using external Bluetooth® devices such as phones and computers (U8). With the exception of components U1 and U8, which must be programmed *prior* to soldering, all components can be programmed or re-programmed *after* being mounted onto the board. Hence, it is recommended that U1 and U8 be soldered onto the PCBs at the very end.

U2 is a Texas Instruments (T.I.) MSP430F2001 microcontroller used to manage the timing and synchronization of the system. It can be programmed using a T.I. MSP-TS430PW28A target board and a T.I. Flash Emulation Tool (F.E.T.) programmer. Using the IAR Embedded Workbench software, the "timerMCU" project code can be downloaded to the MSP430F2001 microcontroller. U8 is a Microchip Technology RN42-I/RM system-on-a-chip (SoC) that is used to broadcast Bluetooth® data. The SoC must be wirelessly programmed to a baud rate of 19,200 by following instructions in the "RN41/42 Evaluation Kit User's Guide" published by Microchip®. Once these devices are programmed, they can be soldered onto their PCBs.

Once the system soldering is complete (Fig. 2), the remaining microcontrollers U3 and U7 can be programmed. Prior to programming, the system must be powered using the detachable battery circuit or other voltage source. Using IAR Embedded Workbench, the data acquisition board and LED control board need to be programmed using the "dataAcquisitionMCU" and "sourceIntensityControlMCU" project codes, respectively.

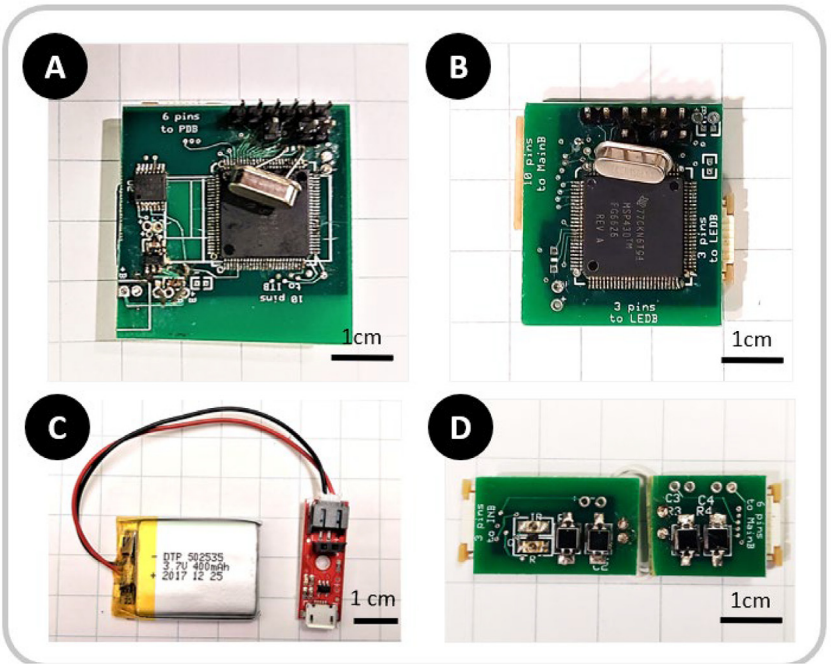

Fig. 2. Images of assembled control circuits. A) Data acquisition and Bluetooth® broadcasting board, B) LED Intensity control board, C) Detachable Sparkfun® LiPo Charger with 400 mAh LiPo battery, D) fNIRS sensing electronics.

Silicone polymer skin

A silicone polymer skin is used to encase the fNIRS sensing electronics into a soft, comfortable, and protective casing that interfaces with forehead skin. The polymer is mixture of a commercially available translucent silicone rubber (Dragon Skin™, BOM: S1) and black-colored color pigment (Silc Pig Silicone Pigment, BOM: S2). This dark liquid polymer mixture, which blocks out ambient light, becomes a flexible solid in the shape of any mold it is provided. The mold was iteratively designed to house the fNIRS sensing electronics in a manner wherein the final LED and photodiode positions are roughly 1 mm away from the head. The polymer mold ensures the fNIRS sensing electronics conform snuggly to the forehead and minimizes movement between the optode and the skin.

The polymer skin preparation process begins by 3D printing the provided mold design. The polymer skin material is prepared (Fig. 3) by mixing an equal amount of the two-part Dragon Skin™ solution (10 g each) by weight (BOM: S1) and 6 drops of a black pigment (BOM: S2). After stirring, the viscous liquid mixture is poured into a 3D-printed mold until the mold is full and is then allowed to cure in air for three hours. To accelerate the curing process, temperature can be elevated, although the mixture will also cure at room temperature. After the mixture is cured, the cured polymer forms a template to fit the fNIRS sensing PCBs with the holes aligned with LEDs and photodiodes on the PCBs. Once the PCBs are correctly aligned and placed in the template, another batch of the silicone-pigment solution (3 g per part, 1 drop) should be poured over the PCBs and left to cure. Note, while pouring the second batch of silicone, the liquid must not rise above the cable connectors at the edges of the fNIRS sensing PCBs. After curing, the assembly needs to be visually inspected to ensure neither the LED nor the photodiode windows were accidentally covered with the polymer. The final system can be wiped clean using rubbing alcohol (70% Ethyl Alcohol).

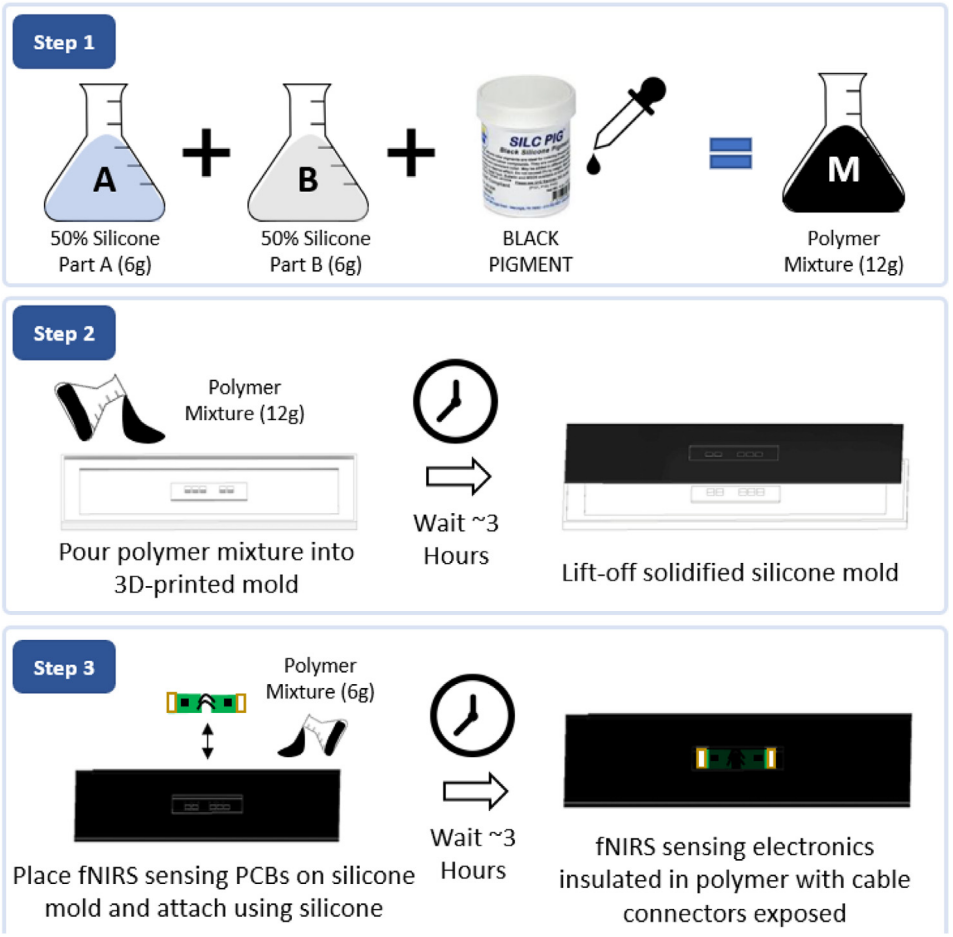

Fig. 3. Silicone polymer skin assembly for insulating and protecting the fNIRS sensing electronics. Step 1) Prepare polymer mixture by mixing equal parts of silicone parts A and B with 6 drops of black pigment. Step 2) Pour silicone and set polymer mold for three hours, then lift-off. Step 3) Place fNIRS sensing electronics on lifted-off silicone mold and set in place using a fresh batch of polymer mixture.

Cloth and Velcro® casing

The final subcomponent is a laser-cut cloth enclosure with a rectangular cut at the center for attaching it to the silicone jacketed fNIRS sensing electronics. Assembly is described in Fig. 4. The cloth cutout will have an overall size of 68 cm × 23 cm, with a rectangular cut-out at the center sized at 7 cm × 5 cm. Although this cut can be achieved without using a laser cutter, a laser cutting file "clothLaserCut" has been provided in the OSF repository. After laser cutting, small 10-cm pieces of 5-cm wide Velcro® need to be sown onto the select locations as shown in Fig. 4. The resulting assembly constitutes a Velcro®-patched cloth that can be attached together into a tube-like formation and wrapped around the head like an adjustable headband.

System consolidation

As described in Fig. 5, the final step for completing the system is to "glue" the polymer-jacketed fNIRS sensing array onto the cloth and Velcro® casing using the same two-part translucent silicone polymer utilized earlier (1 g per part). Using a small spatula, glue is applied to the tapered edges of the polymer-jacketed fNIRS array and pressed down into the cloth. Once the glue has dried, the remainder of the electronics can be assembled. Interfacing the data acquisition and LED-control PCBs with the polymer-jacketed fNIRS sensing array requires two types of FPC cables: one ten-pin cable between the data acquisition and LED boards and two six-pin cables connecting both the data acquisition and LED boards to the sensing electronics board. The data-acquisition board will be connected to the photodiode end of the fNIRS sensing board, and the LED controller board will be connected to the LED source end of the fNIRS sensing board. At the conclusion of the assembly and programming, the LiPo charger circuit can be plugged in to power the board. After the circuit is powered, the two LEDs in the fNIRS electronics will alternatingly pulse, and the data acquisition board will broadcast Bluetooth® data.

11. Operation instructions

The fNIRS headband is very simple to use:

1. Install either interfacing software (the Android App on the phone or MATLAB®/C++ applications on computer) shared in the repositories above. This "installation" process requires prior installation of Android Studio, MATLAB®, or Visual Studio based on the chosen data collection tool.
2. Turn on the fNIRS headband by connecting the detachable battery.
3. Place the fNIRS headband on the forehead of the user and wrap it around the head.

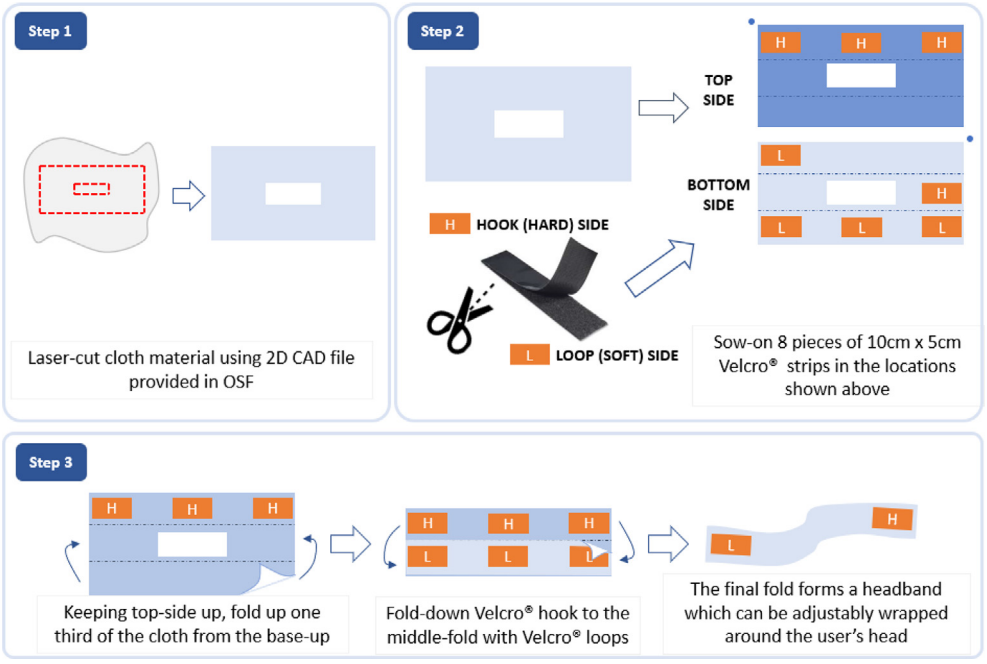

Fig. 4. Cloth enclosure assembly. Step 1) Laser-cut cloth material using the provided "clothLaserCut" file in the OSF repository. Step 2) Sew on Velcro® hook and loop sides to designated areas to form an enclosable headband. Step 3) Fold cloth enclosure to form a "tube" (held together with Velcro®) to be wrapped around the head of a user.

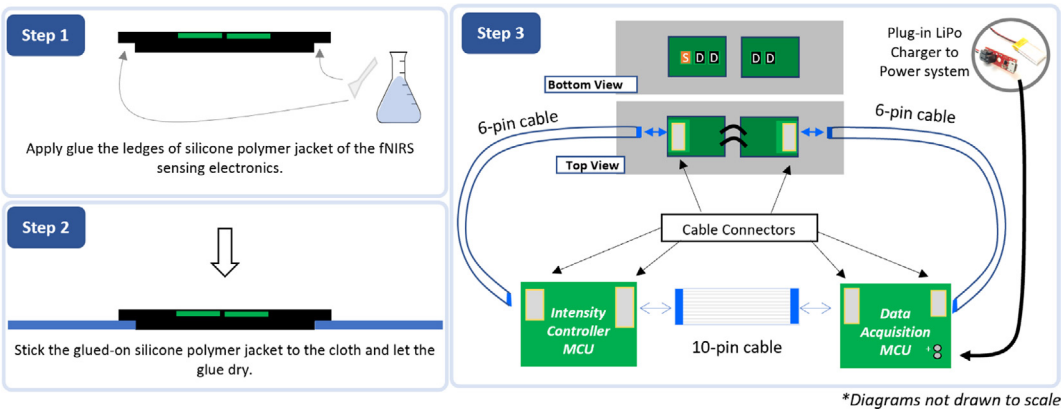

Fig. 5. Consolidation of the remaining components of the fNIRS headband system. Step 1) Apply a small amount of silicone polymer (2 g each of Part A and B) along the tapered edges of the silicone polymer encasing the fNIRS electronics and let dry for three hours. Step 2) Connect flat 6-pin and 10-pin cables as demonstrated in the diagram above to complete assembly of the system. The system can be powered by plugging in the LiPo Charger using the provided female headers.

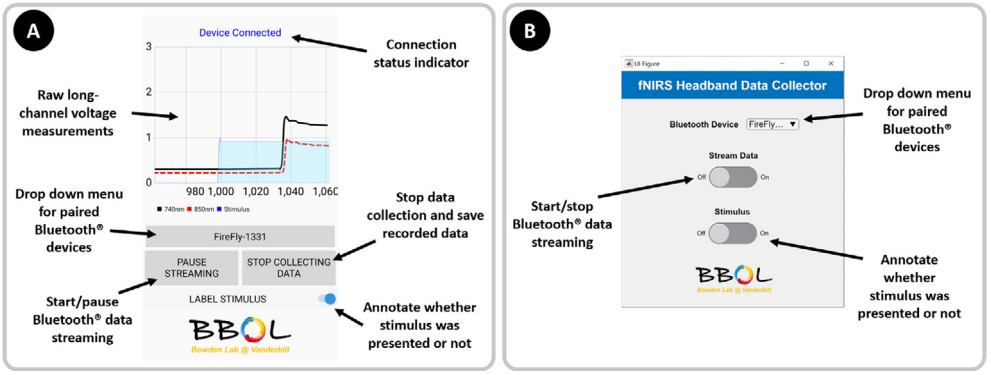

Fig. 6. A) Screenshot of the Android phone application developed using Xamarin.Android. The application allows users to collect raw voltage readings from the fNIRS headband system on the phone for access later. During data collection, users can check the device connection status and annotate data when "stimuli" are applied. B) Screenshot of the MATLAB® computer application to easily connect to and save data from the fNIRS headband system.

4. Pair the fNIRS headband and your device wirelessly using your phone or computer operating system: open your Android phone or Bluetooth®-interfacing computer and select the name of the Bluetooth® module associated with the fNIRS headband on the Android-compatible device.
5. In the interfacing software, select the desired Bluetooth® device from the "drop down menu for paired Bluetooth® devices" of the respective graphical user interface (GUI) in Fig. 6.
6. Press or toggle the "Start/Pause Bluetooth Data Streaming" (Android) or "Start/Stop Bluetooth Data Streaming" (MATLAB®) buttons to start collecting data, and perform experimental activities as desired with the fNIRS headband on (data will be automatically saved locally on the chosen computer or phone). Periods involving a stimulus such as presentation of audio-visual cues or performing neurologically engaging activities can be annotated by toggling the "Label Stimulus" (Android) or "Stimulus" (MATLAB®) buttons shown above.
7. At the conclusion of the experiment, press the button to "Stop data collection and save recorded data" (Android) or simply toggle the button to "Start/Stop Bluetooth® Data Streaming" (MATLAB®). On the Android phone, data will be saved in the "DCIM/NIRS" directory. For the MATLAB® application, data will be saved in the "data" subdirectory of the current project.

12. Validation and characterization

To validate our fNIRS headband device, we acquired hemodynamic measurements during a breath-holding test, an arithmetic test, and resting states with IRB approval.

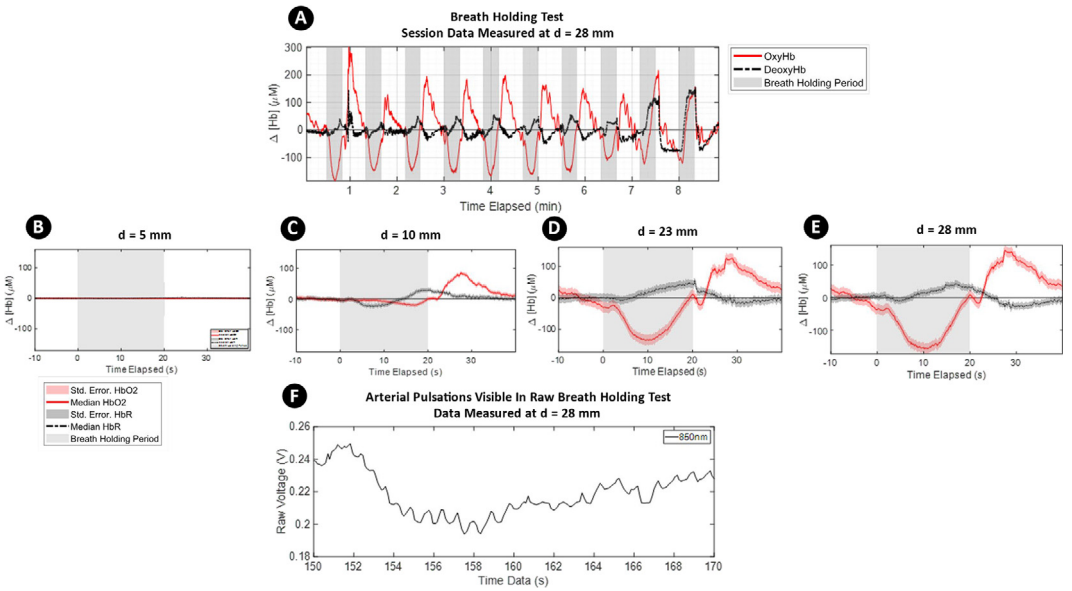

Fig. 7. Physiological validation using a breath-holding test. **A)** Complete session data. The solid red lines represent OxyHb, dashed black lines are DeoxyHb, and shaded gray areas represents breath-holding periods. Characteristic dips and recovery in OxyHb are visible in these data. **B thru E)** Block median with highlighted standard error of the median of 10 cycles measuring the change in baseline measurement with respect to the 10 s preceding the breath-holding period. An increase in source-detector separation results in deeper imaging into the head **F)** A segment of raw, unprocessed data from our fNIRS device during 850-nm LED light input is shown. Arterial pulsations are visible in the figure. (For interpretation of the references to color in this figure legend, the reader is referred to the web version of this article.)

Breath-holding results in a uniform blood oxygenation level dependent (BOLD) response throughout the gray matter of the brain that does not originate from cognitive activity [35,36]. During the experiment, a healthy adult subject was requested to alternate between breathing normally for 30 s and holding their breath for 20 s. Before each breath-holding period, the subject was instructed to take a deep breath. The breathing and breath-holding cycle were repeated 10 times. The results of the experiment are shown in Fig. 7. Fig. 7A shows the complete session data from the experiment. The red curve represents the oxyhemoglobin concentration while the dashed black curve represents the deoxyhemoglobin concentration. These raw voltage data were band-pass filtered (0.05 Hz to 2 Hz) to remove various physiological noises (cardiac, respiratory, Mayer waves) and signal drift. The photodiode readings were then converted to hemoglobin concentrations using the Modified Beer- Lambert Law [37] ($\varepsilon_{Hb,740nm} = 1.1, \varepsilon_{HbO_2,740nm} = 0.45, \varepsilon_{Hb,850nm} = 0.7, \varepsilon_{HbO_2,850nm} = 1.05$). The clear areas in the plot represent normal breathing periods, while the gray background areas represent data collected during breath-holding periods. Block medians (with standard error of the median) of the fNIRS data for the different source-detector separations are shown in Fig. 7B to E. For each figure, 10 s of baseline data before breath holding have been subtracted. It can be observed that as source-detector separation increases, characteristic drops in OxyHb measurements during breath holding periods become more visible, and this trend is reproducible across multiple breath holding cycles. The drop in OxyHb at the onset of breath holding followed by a sharp recovery is consistent with both fNIRS [38–40] and fMRI [41,42] studies and demonstrates that the grey matter of the brain was successfully imaged.

Data from shorter channels, such as those featured in Fig. 7C and D, are typically used by researchers for sensing non-cortical hemodynamic activity and can be subtracted from long-channel data to restrict imaging to cortical activity [10,43,44]. An example of short channel correction can be seen in Fig. 8, which presents results from an arithmetic test. The arithmetic test was conducted for 20 min and consisted of 20 cycles of 30 s of relaxation and 30 s of problem solving. The device was positioned at the F2 location on the forehead of a subject. In Fig. 8A, uncorrected arithmetic test data for the complete 20-minute session are presented. For this duration, a recurrent rise in OxyHb can be observed at the beginning of each problem-solving phase. In Fig. 8B and C, processed data for the short channel at d = 5 mm and long channel at d = 28 mm are shown. Simply subtracting Fig. 8B from 8C gives us 8D: a "short-channel corrected" fNIRS measurement without non-cortical data. While various other methods exist for such short-channel correction [45,46], all such methods serve to remove signal features such as motion or respiratory artefacts unrelated to cognitive activity. The recurrent rise in OxyHb during the problem-solving phase of the arithmetic test correctly reproduces other cognitive load experiments evaluating cognitive load and presents a visible hemodynamic response [47,48]. To demonstrate the stability of the fNIRS measurement, 10-minute and 30-minute resting-state fNIRS measurements of a subject seated on a chair are also shown in Fig. 8E and F, respectively.

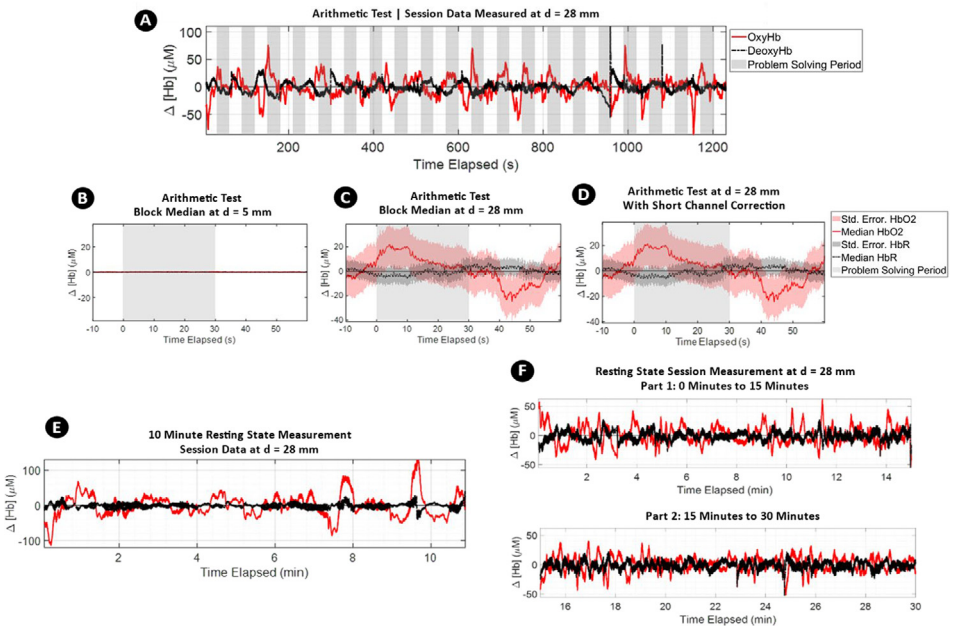

Fig. 8. A) Complete session data of Arithmetic Test. The solid red lines represent OxyHb, dashed black lines DeoxyHb, and shaded gray area represent problem solving periods. Characteristic rises of OxyHb during problem solving phases are visible. **B thru D)** Block median with highlighted standard error median of 20 cycles measuring change in baseline measurement with respect to the 10 s preceding arithmetic problem-solving period. In B and C, change in hemoglobin concentrations are shown from the shortest detector at d = 5 mm and the farthest detector d = 28 mm. In D, the short channel signal from d = 5 mm is subtracted from long channel signal at d = 28 mm to demonstrate short channel correction. **E)** Resting state fNIRS measurements for 10 min. **F)** Resting state fNIRS measurements for 30 min. Both data demonstrate stability of the measurements throughout the imaging durations. (For interpretation of the references to color in this figure legend, the reader is referred to the web version of this article.)

13. Human and animal rights

We have carried out our work in accordance with The Code of Ethics of the World Medical Association (Declaration of Helsinki) and Uniform Requirements for manuscripts submitted to Biomedical journals. This work was conducted under approval of IRB#192103 at Vanderbilt University.

Declaration of Competing Interest

The authors declare that they have no known competing financial interests or personal relationships that could have appeared to influence the work reported in this paper.

Acknowledgement

This work was funded by the Dorothy J. Wingfield Phillips Chancellor Faculty Fellowship and National Institutes of Health (NIH) grant # 1 R21 MH123873-01.

References

[1] P. Pinti, C. Aichelburg, S. Gilbert, A. Hamilton, J. Hirsch, P. Burgess, I. Tachtsidis, A review on the use of wearable functional near-infrared spectroscopy in naturalistic environments, Jpn. Psychol. Res. 60 (4) (2018) 347–373, https://doi.org/10.1111/jpr.12206.
[2] A. Hamilton, P. Pinti, D. Paoletti, J.A. Ward, Seeing into the Brain of an Actor with Mocap and fNIRS, in: ISWC'18 Proc. 2018 ACM Int. Symp. Wearable Comput., 2018: pp. 216–217. DOI:10.1145/3267242.3267284.
[3] T.(舟根司) Funane, H.(敦森洋和) Atsumori, A.(木敦) Suzuki, M.(木口雅史) Kiguchi, Noncontact brain activity measurement system based on near-infrared spectroscopy, Appl. Phys. Lett. 96 (2010) 123701. DOI:10.1063/1.3367737.
[4] R. McKendrick, R. Mehta, H. Ayaz, M. Scheldrup, R. Parasuraman, Prefrontal hemodynamics of physical activity and environmental complexity during cognitive work, Hum. Factors 59 (1) (2017) 147–162, https://doi.org/10.1177/0018720816675053.
[5] K. Izzetoglu, S. Bunce, M. Izzetoglu, B. Onaral, K. Pourrezaei, Functional near-infrared neuroimaging, in: Proc. 26th Annu. Int. Conf. IEEE Eng. Med. Biol. Soc. Vols 1-7, 2004: pp. 5333–5336.
[6] Q. Zhang, X. Yan, G.E. Strangman, Development of motion resistant instrumentation for ambulatory near-infrared spectroscopy, J. Biomed. Opt. 16 (2011) 87008, https://doi.org/10.1117/1.3615248.
[7] B. Khan, C. Wildey, R. Francis, F. Tian, M.R. Delgado, H. Liu, D. Macfarlane, G. Alexandrakis, Improving optical contact for functional near-infrared brain spectroscopy and imaging with brush optodes, Biomed. Opt. Express. 3 (2012) 878–898, https://doi.org/10.1364/BOE.3.000878.

[8] A. von Lühmann, H. Wabnitz, T. Sander, K. Müller, M3BA: a mobile, modular, multimodal biosignal acquisition architecture for miniaturized EEG-NIRS-based hybrid BCI and monitoring, IEEE Trans. Biomed. Eng. 64 (2017) 1199–1210, https://doi.org/10.1109/TBME.2016.2594127.

[9] A. Kassab, J. Le Lan, J. Tremblay, P. Vannasing, M. Dehbozorgi, P. Pouliot, A. Gallagher, F. Lesage, M. Sawan, D.K. Nguyen, Multichannel wearable fNIRS-EEG system for long-term clinical monitoring, Hum. Brain Mapp. 39 (1) (2018) 7–23, https://doi.org/10.1002/hbm.23849.

[10] L. Gagnon, K. Perdue, D.N. Greve, D. Goldenholz, G. Kaskhedikar, D.A. Boas, Improved recovery of the hemodynamic response in diffuse optical imaging using short optode separations and state-space modeling, Neuroimage 56 (3) (2011) 1362–1371, https://doi.org/10.1016/j.neuroimage.2011.03.001.

[11] D. Wyser, O. Lambercy, F. Scholkmann, M. Wolf, R. Gassert, Wearable and modular functional near-infrared spectroscopy instrument with multidistance measurements at four wavelengths, Neurophotonics 4 (2017), https://doi.org/10.1117/1.NPh.4.4.041413.

[12] R.K. Almajidy, U.G. Hofmann, On the design of a multi-channel NIR system to monitor functional brain activity, NIR2013 Proc. (2013) 335–338.

[13] G.E. Strangman, Z. Li, Q. Zhang, Depth sensitivity and source-detector separations for near infrared spectroscopy based on the Colin27 brain template, PLoS One 8 (2013), https://doi.org/10.1371/journal.pone.0066319.

[14] L.A. Dempsey, R.J. Cooper, T. Roque, T. Correia, E. Magee, S. Powell, A.P. Gibson, J.C. Hebden, Data-driven approach to optimum wavelength selection for diffuse optical imaging, J. Biomed. Opt. 20 (2015), https://doi.org/10.1117/1.jbo.20.1.016003 016003.

[15] M.R. Bhutta, K.S. Hong, B.M. Kim, M.J. Hong, Y.H. Kim, S.H. Lee, Note: three wavelengths near-infrared spectroscopy system for compensating the light absorbance by water, Rev. Sci. Instrum. 85 (2014) 2012–2015, https://doi.org/10.1063/1.4865124.

[16] G. Bale, C.E. Elwell, I. Tachtsidis, From Jöbsis to the present day: a review of clinical near-infrared spectroscopy measurements of cerebral cytochrome-c-oxidase, J. Biomed. Opt. 21 (2016), https://doi.org/10.1117/1.jbo.21.9.091307 091307.

[17] F. Lange, L. Dunne, L. Hale, I. Tachtsidis, MAESTROS: a multiwavelength time-domain NIRS system to monitor changes in oxygenation and oxidation state of cytochrome-C-oxidase, IEEE J. Sel. Top. Quantum Electron. 25 (2019), https://doi.org/10.1109/JSTQE.2018.2833205.

[18] R. Holtzer, J.R. Mahoney, M. Izzetoglu, K. Izzetoglu, B. Onaral, J. Verghese, fNIRS study of walking and walking while talking in young and old individuals, Journals Gerontol. - Ser. A Biol. Sci. Med. Sci. 66 A (2011) 879–887. DOI:10.1093/gerona/glr068.

[19] F. Chénier, M. Sawan, A new brain imaging device based on fNIRS, in: Conf Proc. - IEEE Biomed. Circuits Syst. Conf. Healthc. Technol. BiOCAS2007, 2007, pp. 1–4, https://doi.org/10.1109/BIOCAS.2007.4463294.

[20] A. Curtin, H. Ayaz, The age of neuroergonomics: towards ubiquitous and continuous measurement of brain function with fNIRS, Jpn. Psychol. Res. 60 (2018) 374–386, https://doi.org/10.1111/jpr.12227.

[21] H. Obrig, NIRS in clinical neurology a 'promising' tool?, Neuroimage 85 (2014) 535–546, https://doi.org/10.1016/j.neuroimage.2013.03.045.

[22] H. Atsumori, M. Kiguchi, T. Katura, T. Funane, A. Obata, H. Sato, T. Manaka, M. Iwamoto, A. Maki, H. Koizumi, K. Kubota, Noninvasive imaging of prefrontal activation during attention-demanding tasks performed while walking using a wearable optical topography system, J. Biomed. Opt. 15 (2010), https://doi.org/10.1117/1.3462996.

[23] Y. Liu, H. Ayaz, Speech recognition via fNIRS based brain signals, Front. Neurosci. 12 (2018), https://doi.org/10.3389/fnins.2018.00695.

[24] Brite, (1902) 1–2.

[25] A. von Lühmann, C. Herff, D. Heger, T. Schultz, Toward a wireless open source instrument: functional near-infrared spectroscopy in mobile neuroergonomics and BCI applications, Front. Hum. Neurosci. 9 (2015) 617, https://doi.org/10.3389/fnhum.2015.00617.

[26] F. Tsow, A. Bowden, Wearable Functional Near-Infrared (FNIR) Technology and Its Applications in Naturalistic Conditions, 5 (2019). DOI:10.34297/AJBSR.2019.05.000869.

[27] B.B. Zimmermann, D. Tamborini, J. Selb, A. Ortega, D.A. Boas, Development of a Wearable and Scalable fNIRS System, (2019) 104096.

[28] A.C. Merzagora, M.T. Schultheis, B. Onaral, M. Izzetoglu, Functional near-infrared spectroscopy-based assessment of attention impairments after traumatic brain injury, J. Innov. Opt. Health Sci. 04 (03) (2011) 251–260, https://doi.org/10.1142/S1793545811001551.

[29] V. Quaresima, M. Ferrari, Functional Near-Infrared Spectroscopy (fNIRS) for assessing cerebral cortex function during human behavior in natural/social situations: a concise review, Organ. Res. Methods 22 (1) (2019) 46–68, https://doi.org/10.1177/1094428116658959.

[30] T. Yamada, S. Umeyama, A. Kamoshida, Method for leveling the signal-to-noise ratio in multichannel functional near-infrared spectroscopy, Proc. SPIE (2017), https://doi.org/10.1117/12.2250239.

[31] M. Atif Yaqub, Seong-Woo Woo, Keum-Shik Hong, Compact, portable, high-density functional near-infrared spectroscopy system for brain imaging, IEEE Access 8 (2020) 128224–128238, https://doi.org/10.1109/ACCESS.2020.3008748.

[32] OBELAB, Nirsit-Lite Kids Brain Imaging System for Kids, (n.d.). http://obelab.com/upload_file/down/Nirsit-Lite(kids)Brochure-research(eng2020).pdf.

[33] O. Manual, H. Bldg, NIRSIT Operator ' s Manual, 2016.

[34] fNIR BrainSpy 28, (n.d.). https://www.newmanbrain.com/fnir-brainspy-28/.

[35] A.E. Stillman, X. Hu, M. Jerosch-Herold, Functional MRI of brain during breath holding at 4 T, Magn. Reson. Imaging. 13 (6) (1995) 893–897, https://doi.org/10.1016/0730-725X(95)00037-H.

[36] C.R. Idelson, W.C. Vogt, B. King-Casas, S.M. LaConte, C.G. Rylander, Effect of mechanical optical clearing on near-infrared spectroscopy, Lasers Surg. Med. 47 (2015) 495–502. https://www.ncbi.nlm.nih.gov/pubmed/26041069%0Ahttps://www.ncbi.nlm.nih.gov/pmc/PMC4514551/.

[37] Y. Zhao, L. Qiu, Y. Sun, C. Huang, T. Li, Optimal hemoglobin extinction coefficient data set for near-infrared spectroscopy, Biomed. Opt. Express. 8 (2017) 5151–5159, https://doi.org/10.1364/BOE.8.005151.

[38] Choong-Ki Kim, Seungduk Lee, Dalkwon Koh, Beop-Min Kim, Development of wireless NIRS system with dynamic removal of motion artifacts, Biomed. Eng. Lett. 1 (4) (2011) 254–259, https://doi.org/10.1007/s13534-011-0042-7.

[39] M.J. Saikia, W.G. Besio, K. Mankodiya, WearLight: toward a wearable, configurable functional NIR spectroscopy system for noninvasive neuroimaging, IEEE Trans. Biomed. Circuits Syst. 13 (2019) 91–102, https://doi.org/10.1109/TBCAS.2018.2876089.

[40] L. Hirshfield, Development of a Remote-fNIRS Device, (n.d.) 44–60.

[41] Moriah E. Thomason, Brittany E. Burrows, John D.E. Gabrieli, Gary H. Glover, Breath holding reveals differences in fMRI BOLD signal in children and adults, Neuroimage 25 (3) (2005) 824–837, https://doi.org/10.1016/j.neuroimage.2004.12.026.

[42] K. Murphy, A.D. Harris, R.G. Wise, Robustly measuring vascular reactivity differences with breath-hold: normalising stimulus-evoked and resting state BOLD fMRI data, Neuroimage 54 (2011) 369–379, https://doi.org/10.1016/j.neuroimage.2010.07.059.

[43] L. Ga, M. Yucel, D. Boas, R. Cooper, Further improvement in reducing superficial contamination in NIRS using double short separation measurements, Bone 23 (2008) 1–7, https://doi.org/10.1016/j.neuroimage.2013.01.073.Further.

[44] Takanori Sato, Isao Nambu, Kotaro Takeda, Takatsugu Aihara, Okito Yamashita, Yuko Isogaya, Yoshihiro Inoue, Yohei Otaka, Yasuhiro Wada, Mitsuo Kawato, Masa-aki Sato, Rieko Osu, Reduction of global interference of scalp-hemodynamics in functional near-infrared spectroscopy using short distance probes, Neuroimage 141 (2016) 120–132, https://doi.org/10.1016/j.neuroimage.2016.06.054.

[45] M.D. Pfeifer, F. Scholkmann, R. Labruyère, Signal processing in functional near-infrared spectroscopy (fNIRS): methodological differences lead to different statistical results, Front. Hum. Neurosci. 11 (2018) 1–12, https://doi.org/10.3389/fnhum.2017.00641.

[46] Louis Gagnon, Robert J. Cooper, Meryem A. Yücel, Katherine L. Perdue, Douglas N. Greve, David A. Boas, Short separation channel location impacts the performance of short channel regression in NIRS, Neuroimage 59 (3) (2012) 2518–2528, https://doi.org/10.1016/j.neuroimage.2011.08.095.

[47] C. Artemenko, M. Soltanlou, A.C. Ehlis, H.C. Nuerk, T. Dresler, The neural correlates of mental arithmetic in adolescents: a longitudinal fNIRS study, Behav. Brain Funct. 14 (2018) 1–13, https://doi.org/10.1186/s12993-018-0137-8.

[48] E.M. Kurz, G. Wood, S.E. Kober, W. Schippinger, G. Pichler, G. Müller-Putz, G. Bauernfeind, Towards using fNIRS recordings of mental arithmetic for the detection of residual cognitive activity in patients with disorders of consciousness (DOC), Brain Cogn. 125 (2018) 78–87, https://doi.org/10.1016/j.bandc.2018.06.002.

Anupam Kumar is a Ph.D. student in the department of Biomedical Engineering at Vanderbilt University. Prior to this, he attended The University of Texas at Dallas as a Eugene McDermott Scholar, and completed his Bachelor's and Master's degrees in Biomedical Engineering. He is passionate about designing easy-to-use and affordable technologies for low resource settings and aims to pursue future work at the intersections of research and commercialization. His past research experiences have spanned point-of-care biosensors, focused ultrasound therapy, microbiology, implantable neural stimulation, and medical image analysis. His current research interests involve designing device and computer-vision based solutions for low-cost neuroimaging in naturalistic environments.

Audrey K Bowden is the Dorothy J. Wingfield Phillips Chancellor Faculty Fellow and Associate Professor of Biomedical Engineering (BME) and of Electrical Engineering and Computer Science (EECS) at Vanderbilt University. Prior to this, she served as Assistant and later Associate Professor of Electrical Engineering and Bioengineering at Stanford University. Dr. Bowden received her BSE in Electrical Engineering from Princeton University, her PhD in BME from Duke University and completed her postdoctoral training in Chemistry and Chemical Biology at Harvard University. She is a Fellow of SPIE, a Fellow of AIMBE, a Fellow of OSA and a recipient of numerous awards, Her research interests include biomedical optics – particularly optical coherence tomography and near infrared spectroscopy – microfluidics, and point of care diagnostics.

Francis Tsow performed this work as a researcher at the Vanderbilt University. His research interests involve solving real world problems with engineering and scientific solutions. He is interested in applying his training in electrical and bioengineering in identifying and putting together solutions involving multidisciplinary science. In this functional near-infrared spectroscopy (fNIRS) project, he is grateful to have the opportunity to work with the other authors of this paper in developing and validating a standalone, low-cost, and practical fNIRS headband prototype that has the potential to enable other researchers to collect fNIRS data at an unprecedented level. Large-scale collection of fNIRS data in natural environment will afford a new class of big data for machine learning to explore and discover new science and applications, which not only match his overarching interest, but also specifically to his interest in artificial intelligence, which he is actively pursuing.

Hadi Hosseini is an Assistant Professor in the Department of Psychiatry at Stanford University, is the Director of C-Brain Lab (cbrain.stanford.edu) and a member of the Stanford Neuroscience Institute, Maternal and Child Health Research Institute (MCHRI) and Bio-X. He is a computational neuroscientist with a background in electrical engineering. Dr. Hosseini's research involves utilizing advanced multimodal neuroimaging and machine learning techniques to examine connectome-level signatures of psychiatric conditions, and translating those findings for developing noninvasive, personalized interventions to enhance the brain networks in an organic way. He has been using fNIRS for over a decade to examine human brain functioning in naturalistic situations and in treatment settings. He is the MPI on the project funded by National Institute of Mental Health (NIMH) to develop and test a low-cost, wearable fNIRS system for daily monitoring of brain functioning in children with ADHD at home.